Constant Load Testing with In-situ Hydrogen Charging on Martensitic Ultra

Lode Duprez, Muhammad Arafin, Filip Van den Abeele, Nicolas Bernier

ArcelorMittal Global R&D Gent, Zelzate, Belgium

Diego Belato Rosado

Universidade Federal do Rio Grande do Sul - UFRGS - PPGE3M, Brazil

Jonas De Mey, Veronique Van Speybroeck

Center for molecular modeling, Ghent University, Technologiepark 903, 9052 Gent, Belgium

Abstract

In this work the hydrogen embrittlement of a UHSS martensitic steel was tested by means of the constant load testing method on notched tensile samples with in-situ cathodic hydrogen charging. As the method was developed to screen and compare various steel grades, charging conditions were chosen in such a way that rupture was obtained on a short time scale, i.e. of the order of minutes. Samples were tested at various levels of the nominal stress, i.e. from 550 MPa to 1200 MPa. Detailed data analysis was combined with finite element simulations of the stress state ahead of the notch in order to obtain a correct insight in the mechanical behaviour. Afterwards, interrupted tests were performed and the samples were retained for in-depth characterisation by means of EBSD to get a first insight in the crack propagation mechanisms.

Keywords

Hydrogen embrittlement, constant load testing, martensitic steel, notched tensile samples, interrupted testing, finite element simulation, crack propagation path.

Contact

lode.duprez@arcelormittal.com

Introduction

Carbon steels can be confronted with hydrogen in a variety of situations, e.g. hydrogen induced cracking (HIC) and sulphide stress corrosion cracking (SSCC) in steel pipes, fish scale formation in enamelling grades, hydrogen embrittlement of welds, delayed fracture in high strength steel grades, hydrogen induced fracture of electro-coated fasteners made of quench and tempered steels, hydrogen induced disbonding of claddings.

When it comes to hydrogen embrittlement, for each situation, the boundary conditions will be different, e.g. applied stress levels (next to the residual stresses), absorbed H contents, corrosive attack, fatigue loading, etc. Next to the environmental conditions, the potential hydrogen issues will depend on the steel grade used for the respective application conditions. For example:

- Multiphase, thin gauge ultra high strength steels (UHSS) with tensile strength levels well above 1000 MPa can sometimes suffer from hydrogen induced delayed fracture due to the hydrogen pick-up via e.g. corrosion or during electrodeposition of metallic coatings [1-3]. Minimising the H-uptake and optimising the hydrogen resistance of the steel's microstructure are essential measures to prevent delayed fracture. It is important to note that in the case of electro-coated products, a finite amount of hydrogen is provided by the coating process, which means that adequate trapping may be a very effective way to improve the steel's resistance to hydrogen.
- Microalloyed, hot rolled pipeline grades for oil and natural gas transport can suffer hydrogen induced cracking (HIC) or sulphide stress corrosion cracking (SSCC) due to the enhanced hydrogen pick-up from H_2S containing environments [4-7]. Minimising segregation and formation of elongated MnS are only two of the many requirements to control these phenomena. In contrast to the first example, in this case the source of hydrogen supply is infinite, which makes the conception of a microstructural solution much more complex.

Mechanical evaluation of the hydrogen embrittlement in thin gauge UHSS is not straightforward. Common techniques to visualise the hydrogen effect is by performing slow strain rate testing (SSRT) or constant extension rate testing (CERT), or constant load testing (CLT) in tensile mode. For the first, a sensitivity factor to hydrogen embrittlement can be defined as the procentual loss in tensile ductility or reduction of area between tests performed in air and tests performed with in-situ hydrogen charging. The sensitivity factor is however very depending on the applied charging conditions. For the constant load testing, a time to rupture is determined for various applied stress levels. The various aspects of this test are discussed in this contribution.

In this work an ultra high strength martensitic steel was characterised by the constant load method using notched tensile samples. The objective was to evaluate the constant load methodology by obtaining a better understanding of all phenomena that occur during constant load tests and the mechanisms that influence the final fracture. Therefore the obtained mechanical results are discussed and interpretated using finite element calculations. In addition, samples obtained from interrupted constant load tests were characterised in detail for profound understanding of the crack growth in the investigated martensitic steel.

Experimental

Material

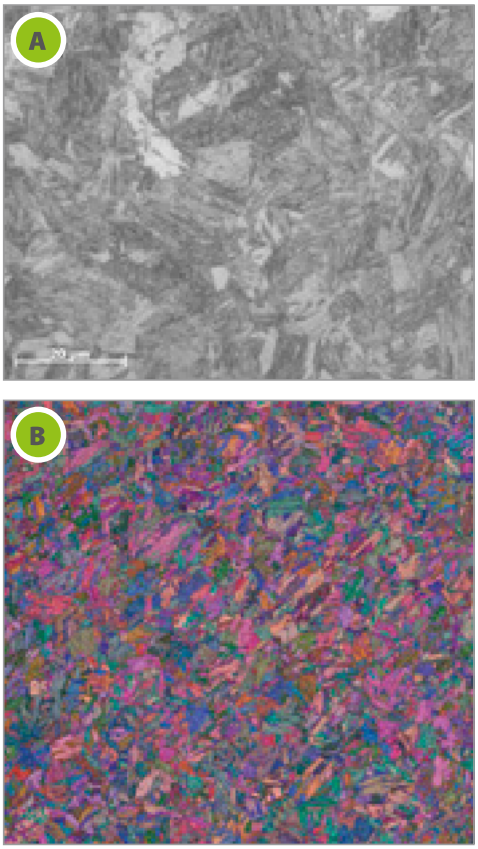

Figure 1: (a) Optical microstructure of the investigated fully martensitic steel. (b) For comparison, the Euler angle mapping, as obtained via EBSD, is shown.

The chemistry of the investigated steel is shown in Table 1. Essentially, the steel has a very lean chemistry with only minor alloying additions. The optical microstructure of the investigated steel, as obtained after nital etching is shown in Figure 1. The microstructure is fully martensitic, which results in a strength level of 1364 MPa in the rolling direction, with only limited ductility, Table 2. The material was processed via classical hot rolling, cold rolling, and a subsequent thermal treatment consisting of austenitising and quenching.

C	Mn	Si	Ti+Nb+V	Cr+Mo+B
0.17	<1%	< 0.5%	< 0.1%	< 0.5%

Table 1: Chemistry of the investigated martensitic steel, in weight percent.

$Rp_{0.2}$ MPa	R_m MPa	A_{80} %
1149	1364	4.5

Table 2: Mechanical properties of the investigated martensitic steel (in the rolling direction)

Notched tensile samples

The samples used for the constant load tests had a width of 12.5 mm and a thickness of 1.5 mm. The length of the samples was taken in the rolling direction of the material. A notch was prepared as shown in Figure 3, with a radius of 0.5 mm. At the notch position, the remaining sample width was 10 mm. All samples were grinded and sandblasted in order to remove all surface oxides.

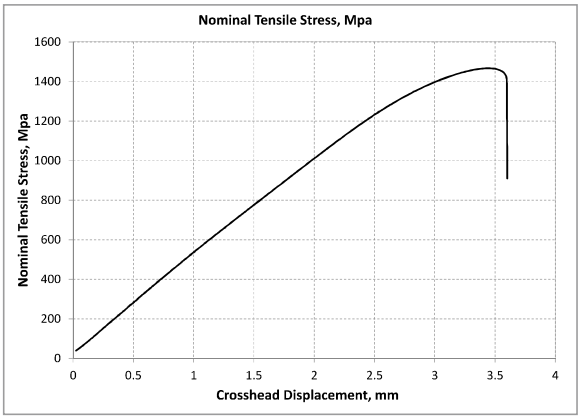

Figure 2: Nominal stress vs crosshead displacement for the investigated martensitic steel, when tested in air at 5 mm/min, using a notched tensile sample geometry.

Tensile tests were performed in air, on the notched samples, in order to obtain an idea of the strength level in the presence of a notch. A typical "nominal stress vs. crosshead displacement" curve is shown in Figure 2. The nominal stress is defined as

$$\sigma_{nom} = \frac{F}{A_{notch}} \qquad (1)$$

with F the applied load (in N) and A_{notch} the original section area at the notch position (in mm^2).

Based on this particular "stress-displacement" curve, it was decided to

perform constant load tests at nominal stress levels from 1200 MPa down to 550 MPa.

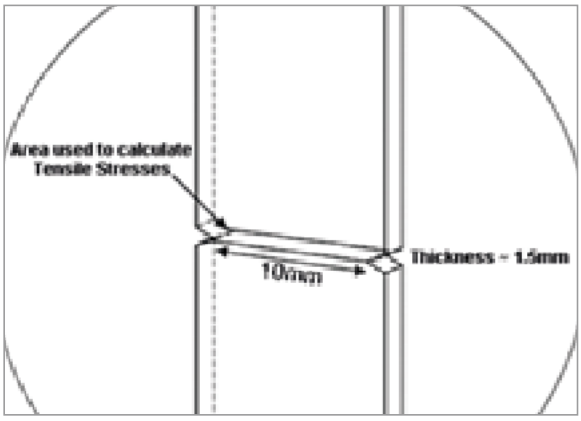

Figure 3: Schematic illustration of the notched tensile sample geometry

Charging conditions during constant load testing

The charging solution was a water based solution containing 27.47 ml H_2SO_4 per 1 l water. Additionally, thiourea was added to poison the hydrogen recombination reaction. The notched tensile samples were mounted in a glass cell, which was filled with 1.75 l of charging solution. Subsequently, samples were precharged galvanostatically during 60 min at a current density of 1 mA/cm^2, using a platinum anode. Internal experience has shown that these charging conditions result in a total hydrogen content of about 4-5 ppm, when samples are charged without mechanical solicitation. Hence, these charging conditions were rather hard, which was done intentionally in order to accelerate the constant load tests and allow for faster screening of materials. It was verified that no blisters occurred after the testing, as this would lead to wrong interpretation of the mechanical results.

After the precharging, the constant load was applied, using a strain rate of 5 mm/min. Once the targeted nominal stress level was achieved, the load was kept constant and H-charging continued at the same current density until rupture occurred.

Crack propagation study

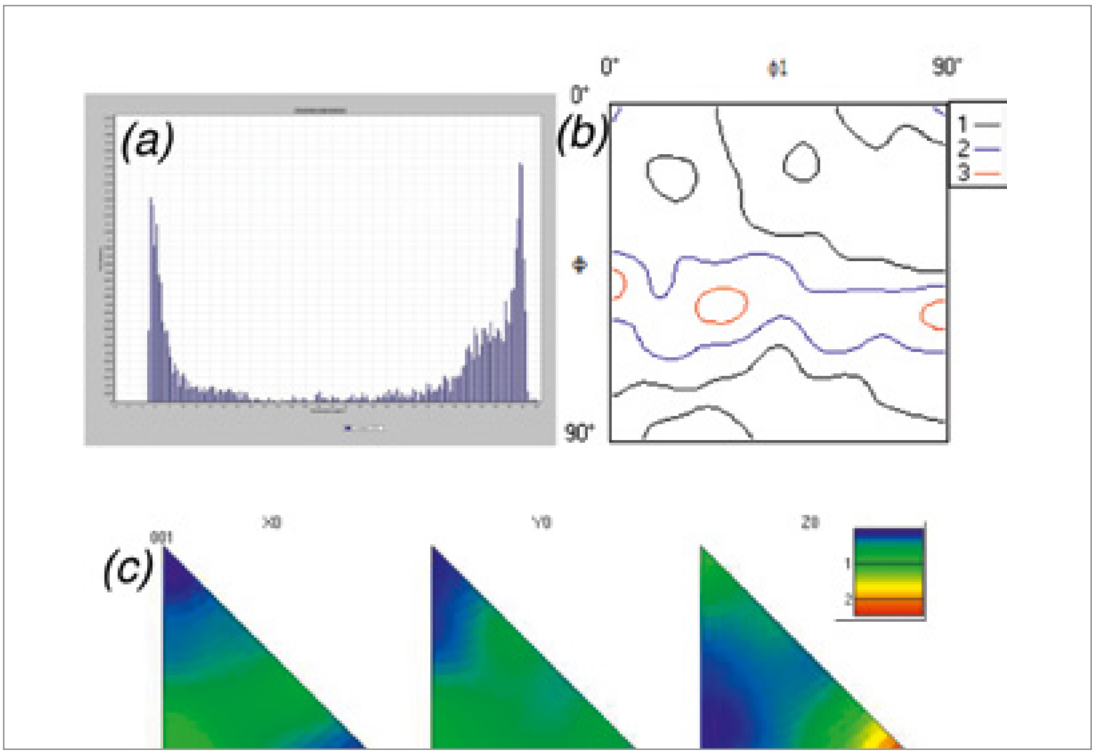

Figure 4: (a) Misorientation angle distribution profile, (b) ODF section at j2 = 45°, and (c) Inverse Pole Figure (IPF) along X0 (=RD), Y0 (=TD) and Z0 (=ND) corresponding to the EBSD mapping shown in Figure 1.

Electron Backscatter Diffraction (EBSD) [8] experiments have been carried out on a Jeol JSM-7001F FEG-SEM equipped with a HKL/Nordlys detection system. Special attention was paid to avoid any structural deterioration during the sample preparation, e.g. only very soft cloth plates were used for polishing the sample. A final mechanical and chemical polishing step using a colloidal silica suspension was performed for 3 minutes just before the EBSD analysis to remove the damaged layer at the top surface of the sample. The data post-treatment was performed using the HKL Channel5 program, especially a noise reduction of mappings. The sample orientation was the same for all mappings, i.e. the transversal direction (TD) and the rolling direction (RD) respectively vertically and horizontally aligned. The normal direction (ND) is therefore normal to the analyzed surface.

An EBSD mapping was first acquired far from the crack to examine the bulk microstructure in the investigated steel. Figure 1(b) gives evidence of a block martensitic structure with a mean grain size measured at 2.9 µm using a critical misorientation angle of 5°. The grain boundary misorientation profile shown in Figure 4(a) is typical for a martensitic sample [9-10] with two peaks at around 5-10° for low-angle martensitic grain/packet boundaries and at around 55-60° mostly for high-angle block boundaries. The orientation distribution function (ODF) section at j_2 = 45° in Figure 4(b) proves the existence of a fibre texture {111}<uvw> with a reinforcement for the {111}<112> components. The inverse pole figures (IPF) along the main specimen axes in Figure 4(c) confirm the presence of a high amount of ND//<100> oriented grains, combined with a RD mostly oriented between the <110> and <112> directions.

Results and discussion

Constant load tests

The results of the constant load tests are shown in Figure 5. For the high applied nominal stresses, the rupture times are very short, i.e. samples break in the order of minutes. This is certainly due to the aggressive charging conditions, causing very fast fracture of the samples.

Further, it is clear that lower applied nominal stresses induce longer "times to rupture". Below a certain nominal stress magnitude (650 MPa) the times to rupture increase sharply. Apparently, there is a so-called threshold stress below which the failure occurs very slowly. This threshold value is not a pure material parameter, as the authors observed that it was also influenced by the charged H-content. As indicated schematically in Figure 5, it was observed for several martensitic grades that by lowering the charged H-content, i.e. reducing the cathodic current density, the times to rupture shifted to higher values (i.e. to the right) and the threshold value increased. This is confirmed by the work of other authors[11], who performed constant load tests at one nominal stress with various charged H-contents. They found a

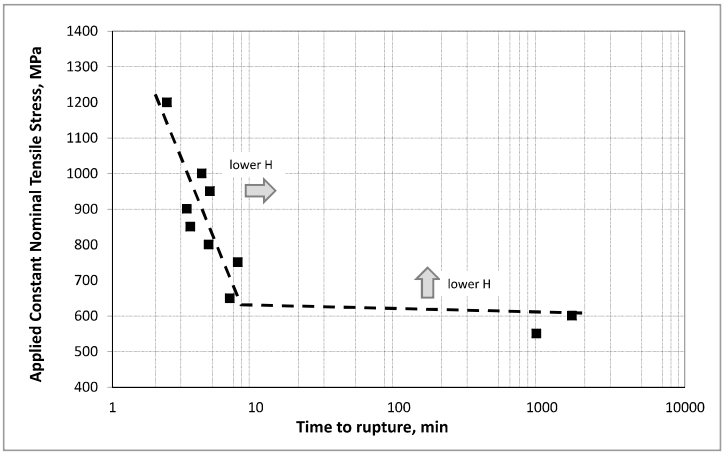

Figure 5: Effect of applied nominal stress on the failure time for the investigated martensitic steel. Note the abrupt increase of failure time at 550 MPa loading.

similar dependency as in Figure 5, only with the charged H-content as Y-axis instead of the applied nominal stress. In this way, they indicated that for a certain applied stress level, there was a critical hydrogen content below which the times to rupture increased dramatically.

Finite element simulations

The above observations require further investigations and clarifications, and a better understanding of the stress field around the notch tip area is the logical first step for this purpose because a plastic zone will exist in this area due to the stress concentration effect. The failure time is expected to be dictated not only by the magnitude of the stress level but also by the diameter of the plastic zone immediately ahead of the notch-tip. Transport of diffusible hydrogen to the high stress concentration area, which in turn is governed by both the available hydrogen and stress magnitude, will further contribute to the reduced failure time or, in other words, lower the threshold stress.

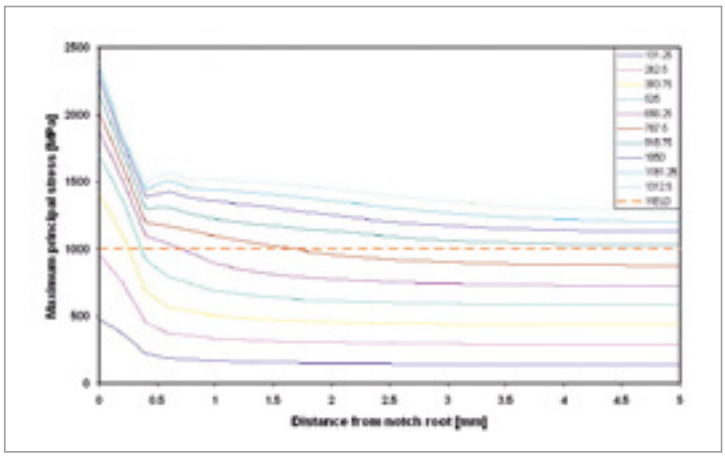

Figure 6: Maximum principal stress distribution across the specimen half-width for various applied stress magnitudes

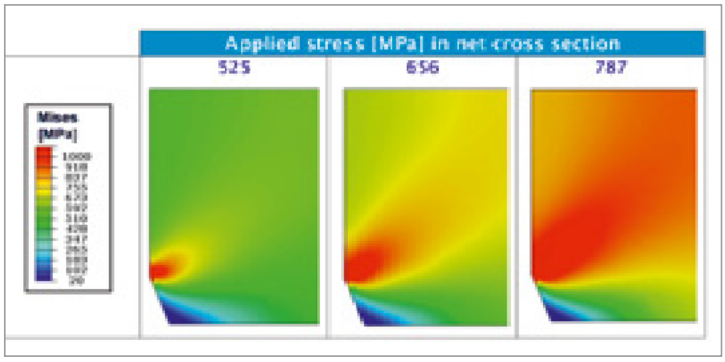

Figure 7: Sharp increase of plastic zone with the increase of applied stress magnitudes (525 – 787 MPa, interval 131 MPa)

To evaluate the stress field around the notch-tip area, finite element modeling (FEM) was carried out for the given specimen geometry and the results are presented in Figure 6. It can be clearly seen that maximum principal stress can easily exceed the yield stress for an applied stress level as low as 270 MPa. However, when observed carefully (see also Figure 7 for a better visualization of the stress fields around the notch for three different stress magnitudes), it can be noticed that

- above ~525 MPa, the distance over which the stress exceeds the yield value increases sharply
- above ~656 MPa, this increases even more rapidly
- beyond 787 MPa, the entire cross-sectional area is above the yield level. This may justify the observed quick failure of the specimens for an applied stress magnitude of ≥ 650 MPa.

While the FEM calculations indicate that the very short failure time should probably correspond to an applied stress of above 650 MPa, the experimental results suggest a somewhat lower value (≤650 MPa). However, this discrepancy is not surprising because the hydrogen effect was not considered in the present calculation. Nevertheless, the

trend in Figure 6 clearly explains the dramatic increase of failure time below a given stress magnitude.

To account for the effect of hydrogen, the local accumulation of hydrogen ahead of the notch-tip can be estimated using the following equation, as proposed by Wang et al. (2005) [12]

$$H = H_D \exp\left[\frac{-M_H(\sigma_h - \sigma_{h,\min})}{RT}\right] \quad (2)$$

Where, H is the locally accumulated hydrogen concentration, H_D is the amount of diffusible hydrogen, σ_h is the hydrostatic stress ahead of the notch-tip, $\sigma_{h,min}$ is the hydrostatic stress far from the notch, M_H is the partical molar volume of hydrogen, R is the gas constant, and T is the test temperature. These calculations are currently ongoing and will be reported shortly.

Interrupted testing

When analysing the data logged during the constant load test, more information can be extracted. As shown in Figure 8, after the initial crosshead displacement, which is related to the application of the constant load, the displacement does not remain constant but very soon continues at a very slow rate.

The interpretation of the continuous displacement is discussed further, but the following observations were made repeatedly:

- At the intermediate stages of the test, in many experiments the displacement rate a was almost constant during a certain time interval. In the later stages the displacement rate increased with the time of loading, the increase becoming more important in the final stages of the experiment, followed by final fracture.
- a was found to be very depending on the applied nominal stress level. More specifically, the displacement rate a increased with increasing applied nominal stresses. More work is ongoing to correlate the a-parameter with the time-to-rupture graphs (cfr. Figure 5) and the material parameters, with the final goal to compare various materials.

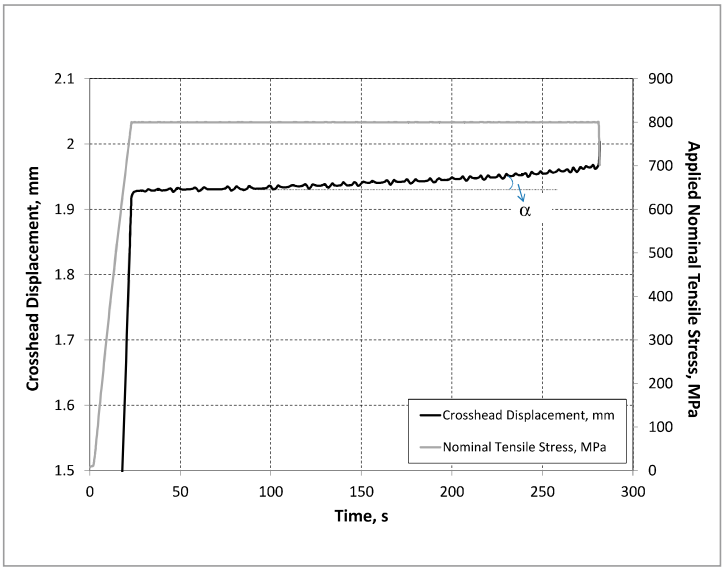

Figure 8: Crosshead displacement and applied nominal stress evolution in time during constant load testing with in-situ hydrogen charging. As can be seen, very soon after reaching the targeted constant load, continuous deformation (as visualised by a crosshead displacement) occurs, as illustrated by the slope α.

For better understanding of the phenomena that occur during the constant load test, experiments were stopped before the final fracture, and the samples were investigated more in detail. Immediately, it became clear that one or more cracks were initiated at the bottom of the notch, Figure 9. In some cases, a clear plastically deformed area could as well be seen.

This observation has some consequences for the interpretation of the constant load test on notched tensile samples:

- Finite element simulations as shown in Figure 6 and Figure 7 are only valid for the initial situation and can consequently only be used to get an indication of the stress concentrations at the start of the test. Once a crack is initiated, the stress and strain state ahead of the notch will alter significantly, and a fracture mechanics approach becomes necessary.
- The observed displacement rate a probably visualises the crack initiation and propagation. Currently, it is not clear when the initiation exactly takes place and what the relative contribution is of the initiation and propagation stage in the test.
- Once a crack is initiated, the cross-sectional area will decrease. Hence, while the applied nominal stress remains constant (as it is calculated as the applied load divided by the original section), the actual average stress levels will increase, which as such will increase the mechanical sollicitation. This can already cause an acceleration of the damage phenomena that occur, which might explain partially the increasing a-parameter.

Figure 9: Some examples of crack appearance during the constant load testing.

In relation with this crack propagation, it is interesting to indicate that fracture surfaces of the broken samples showed a specific aspect, which is function of the applied nominal stress level. Whereas the centre of the broken sample often showed a ductile fracture, more brittle-like aspects were mainly observed at the notch root, as shown in Figure 10. Concerning this brittle area:

- The size of this brittle area seemed to be dependent on the applied stress level, i.e. for the highest nominal stresses (i.e. the shortes test times), the brittle area had a limited size. For the lowest stress levels, i.e. around the threshold, this brittle area had a distinctively larger size.
- The correlation between the various zones on the final fracture surface and the crack initiation and propagation phase are currently under investigation.
- Regularly, this brittle area had a triangular shape, i.e. the brittle zone reached much higher depth in the centre of the sample than in the surface area. Possibly, preferred brittle fracture might be induced in the hard centerline bands, which are known to originate from segregation phenomena.

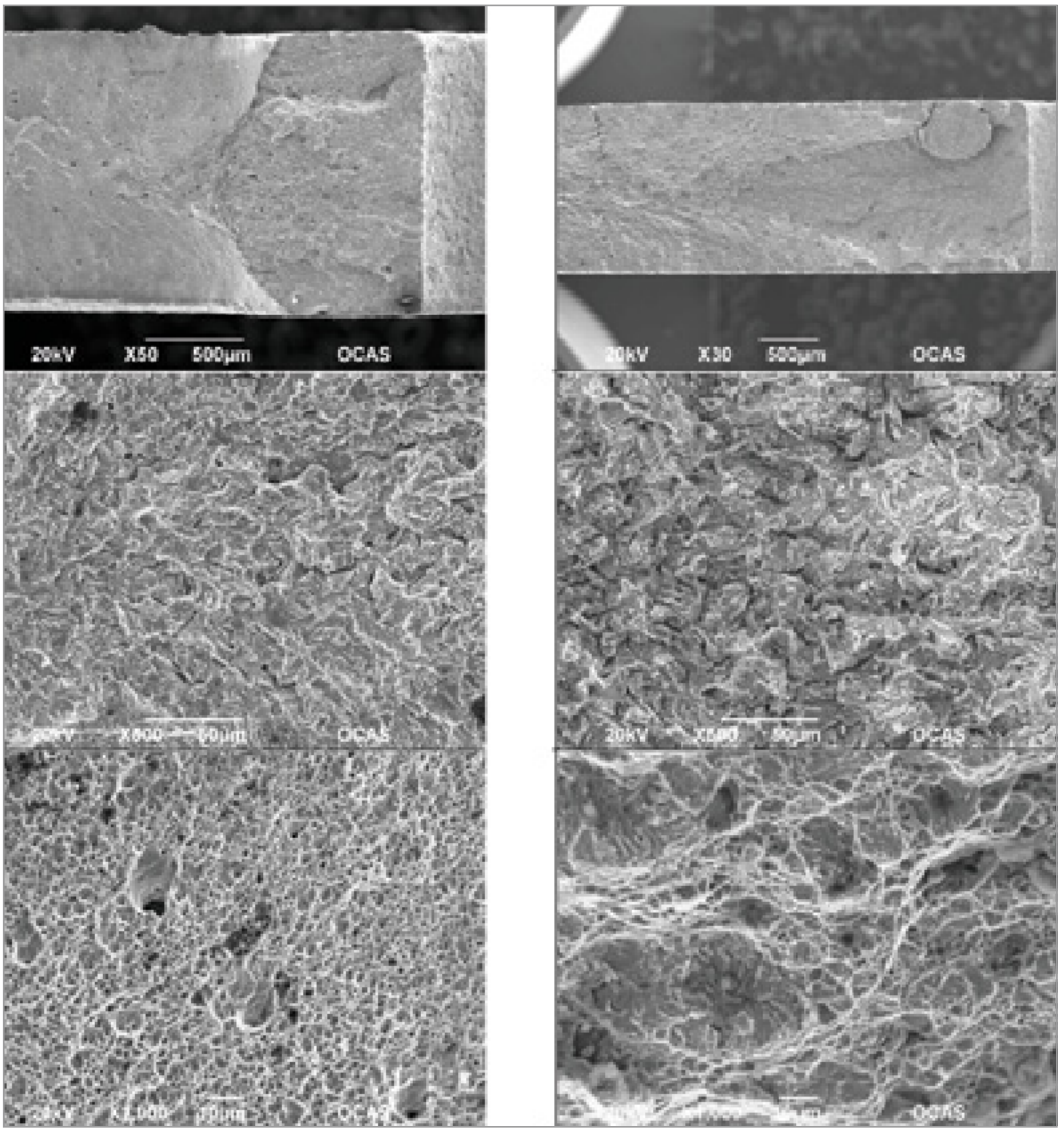

Figure 10: Fracture surfaces as observed on broken samples0. Left images correspond to the sample tested at 850 MPa, broken after 3.4 minutes. The right column shows the fracture surfaces of a sample tested at 600 MPa, that broke after 844 minutes. The top image is an overview image with the notch being situated at the right side of the image. The middle image illustrates the fracture surface just below the notch root, whereas the bottom images correspond to the middle of the sample.

Crack investigation

The verification of a possible correlation between 'microtexture' (i.e. texture at the scale of the grain size) and crack propagation may be essential for the understanding of a steel grade's sensitivity to H embrittlement. Therefore EBSD was performed on the steel loaded under H charging at a constant stress of 800 MPa for 120 seconds. As mentioned above, this interrupted test allows the formation of cracks in the material while preventing it from being totally ruptured.

For the investigation of the crack initiation, EBSD mappings were taken in several areas close to the notch and at different thickness levels. Two representative mappings are shown in Figure 11 with the notch located at the bottom. For determining the type of cracking mode, the disorientation angle between two surrounding zones was measured as indicated by the red arrow in Figure 11(a). Results show that this disorientation angle is regularly smaller than 5° for mappings close to the notch, i.e. only transgranular (TG) cracks are propagating. Since the total crack length extends to distances much larger

than the EBSD scanned area, some parts of the crack are not analyzed which renders the measurement of the length of the pure TG zone very inaccurate. It has to be noticed that cracks exhibiting a mixed transgranular - intergranular (TG-IG) mode from the notch were all stopped very fast, e.g. cracks on the left-hand side in Figure 11(a) and on the right-hand side in Figure 11(b) have a length smaller than 100 µm (red circles in Figure 11 surround the crack tips).

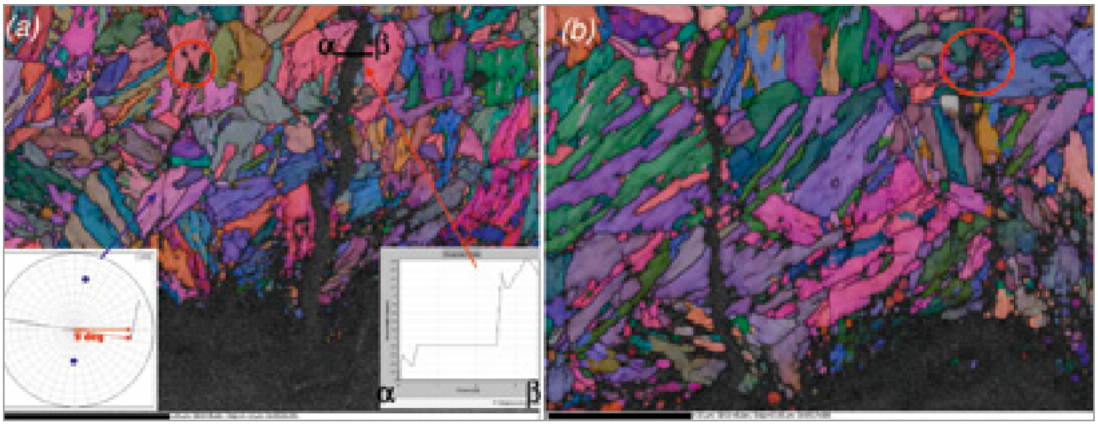

Figure 11: EBSD mapping on the cracked region close to the notch at two different locations. The disorientation angle profile from points a to b allow the type of cracking mode to be determined. The red circles indicate the tip of very short crack exhibiting a mix TG-IG cracking mode.

The knowledge of the cracking plane is of utmost importance but its determination only from one EBSD mapping is impossible as the angle between the sample surface and the cracking plane is not known. In this study, the approach proposed in [13] is used to estimate the probability that cracks are propagating along {001} planes. It consists in comparing the trace of the crack at the surface of the sample with the trace of the plane normal to one of the <001> directions of the cracked martensitic packet. It is found that for most of the grains, the trace of the crack is parallel to the normal to the projection of a <001> direction; e.g. in the insert of Figure 11, the projection [14] from the cracked grain indicated by the blue arrow gives a trace of {100} planes at an angle of 9° from TD, very close to the angle between TD and the trace of the crack in this grain.

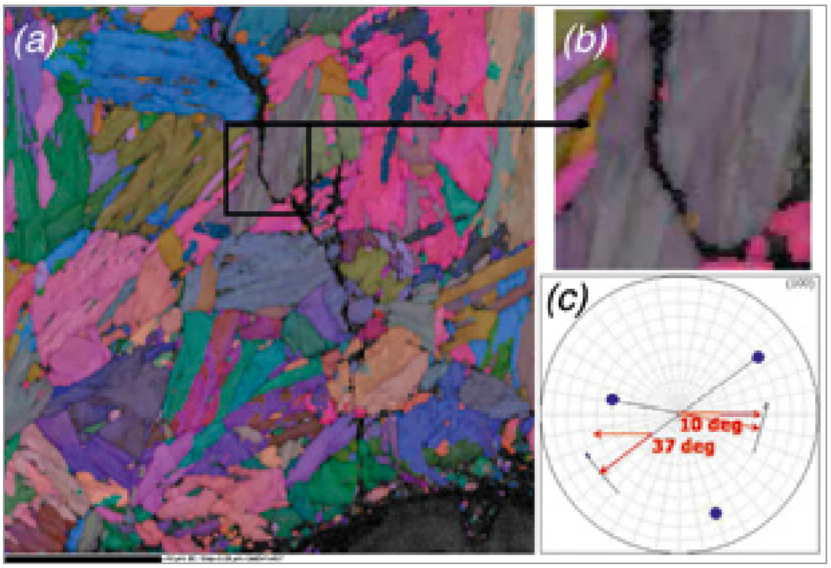

Figure 12: (a) EBSD mapping of a cracked region close to a notch, (b) zoom on a particular grain in which the crack is deviated by a block boundary, (c) <100> projections of the grain displayed in (b) indicating most likely {100} cleavage planes for both directions.

The pure TG mode close to the notch is confirmed in a third EBSD mapping displayed in Figure 12(a). Similarly to the previous EBSD mappings, the crack path is mainly deviated as soon as a grain/packet boundary is encountered, i.e. the crack generally follows one unique direction in each martensitic packet. A few grains exhibit however several crack directions, e.g. in the martensitic packet shown in Figure 12(b). In this situation, the crack is abruptly deviated by a block boundary, and is subsequently propagating between two blocks. It is interesting to note that both directions of the crack are a priori compatible with {001} cleavage planes, as can be seen in the <001> projections in Figure 12(c). Note that the orientation of high-angle block boundaries, known as sensitive to intragranular cracking [15], parallel to the direction of tensile loading may also affect the crack deviation in the grain.

Further away from the notch, disorientation angles between surrounding zones of the crack lie within two main ranges: smaller than 5°, and between 20° and 45°. These values imply the presence of both TG and intergranular (IG) cracking modes. However, it is well known for martensite that the orientation relationship (OR) between parent austenite and martensitic laths follow both Kurdjumov–Sachs (K–S) and Nishiyama–Wassermann (N–W) OR which cover boundary angles smaller than 20° and larger than 45° [9-10]. Therefore, grain boundaries exhibiting deviation angles between the two latter values allow most of the former austenite grain boundaries to be highlighted. Figure 13 gives evidence of the superimposition of the crack path with former austenite grain boundaries (drawn in bold blue contours) in the different IG regions indicated by green arrows.

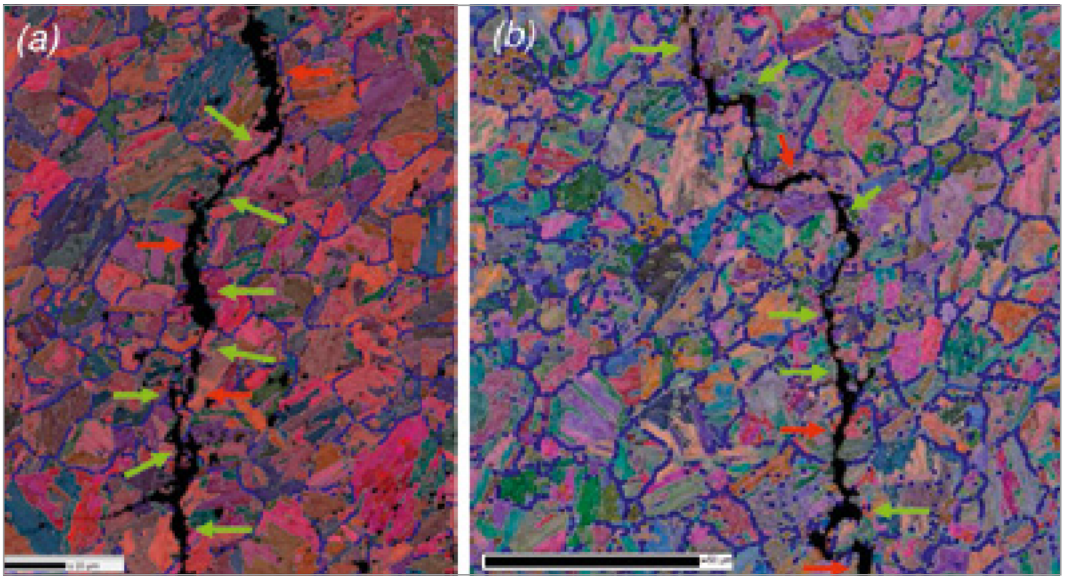

Figure 13: EBSD mappings acquired in two different areas further away from the notch. IG cracks (with some indicated by green arrows) are regularly propagating along former austenite grain boundaries (i.e. between 20° and 45° represented by bold blue lines). Red arrows point to TG cracks.

As a final comment, the texture of grains surrounding the cracks has been calculated for every mapping and compared to the global texture of the base material shown in Figure 4. Results show that there is neither a clear difference with the overall texture, nor a clear trend for grain orientations particularly subject or insensitive to cracking. In summary, the grain orientation has a very low impact on the crack propagation.

Conclusions

In this work the hydrogen embrittlement of a UHSS martensitic steel was tested by means of the constant load testing method with in-situ cathodic hydrogen charging. As the method was developed to screen and compare various steel grades, charging conditions were chosen in such a way that rupture was obtained on a short time scale, i.e. the order of minutes. Samples were tested at various levels of the nominal stress, i.e. from 550 MPa to 1200 MPa.

Rupture times (when plotted on a logarithmic scale) were found to increase almost linearly for decreasing applied loads, with a threshold stress level between 600 MPa and 650 MPa below which the linear relation was not longer followed and the material resisted to the applied load for much longer times.

First finite element calculations were done to get a better understanding of the fundamental causes of this threshold value.

Detailed analysis of the evolution with time of the crosshead displacement learned that during the constant load test the material experienced almost continuous deformation.

Interrupted tests with subsequent analysis showed that that cracks occured rapidly at the root of the notch and propagated until a critical size was obtained, followed by rapid final fracture. The exact monitoring of the crack initiation and subsequent propagation stage is still under investigation.

A crack investigation by means of EBSD was performed on a sample obtained from an interrupted constant load test at 800 MPa. The results indicate that two parts can be distinguished along the crack path: one part close to the notch for which transgranular cracking predominantly exists, and a second one extending up to the crack tip where both transgranular and intergranular cracks can be noticed.

Transgranular cracks are very likely propagating along the {001} planes in every martensitic packet, whereas intergranular cracks mostly follow the former austenite grain boundaries. Observation of the fracture surface confirms the presence of both brittle and ductile cracking modes in the material.

References

[1] Ji Soo Kim, You Hwan Lee, Duk Lak Lee, Kyung-Tae Park, Chong Soo Lee; Microstructural influences on hydrogen delayed fracture of high strength steels; Materials Science and Engineering A 505 (2009) 105–110

[2] Kunio NAMIKI, Kenji ISOKAWA; Effect of Sulphur Content on Delayed Fracture Susceptibility of High Strength Steel for Bolts; Transactions ISIJ, Vol. 24, 1984; pp. 567

[3] G. Lovicu, M. Barloscio, M. Bottazzi, F. D'Aiuto, M. De Sanctis, A. Dimatteo, C. Federici, S. Maggi, C. Santus, R. Valentini; Hydrogen Embrittlement of Advanced High Strength Steels for Automotive Use

[4] Hardie D, Charles EA, Lopez AH. « Hydrogen embrittlement of high strength pipeline steels" Corrosion science 2006; 48: 4378-4385.

[5] B.E. Wilde, C.D. Kim, E.H. Phelps, Corrosion 36 (1980) 625.

[6] G. Domizzi, G. Anteri, J. Ovejero-Garcia, Corrosion Science 43 (2001) 325.

[7] C.F Dong, Z.Y. Liu, X.G. Li, Y.F. Cheng. Effects of hydrogen-charging on the susceptibility of X100 pipeline steel to hydrogen-induced cracking. International journal of hydrogen energy 34 (2009) 9879-9884.

[8] Introduction to Texture Analysis: Macrotexture, Microtexture and Orientation Mapping by Valerie Randle, Publisher: CRC Press; 1 edition (August 7, 2000)

[9] S. Morito, X. Huang, T. Furuhara, T. Maki, N. Hansen, The morphology and crystallography of lath martensite in alloy steels ,Acta Materialia 54 (2006) 5323–5331

[10] Electron backscattering diffraction study of acicular ferrite, bainite, and martensite steel microstructures, Gourgues A.-F; Flower, H.M; Lindley, T.C., Materials Science and Technology, Volume 16, Number 1, January 2000 , pp. 26-40(15)

[11] J.S. Kim, Y.H. Lee, D.L. Lee, K.T. Park, C.S. Lee.Microstructural influences on hydrogen delayed fracture of high strength steels, Materials Science and Engineering A 505 (2009), 105-110

[12] Wang, M., Akiyama, E., Tsuzaki, K. (2005) Effect of hydrogen and stress concentration on the notch tensile strength of AISI 4135 steel, Mater. Sci. Eng. A., 398, 37-46.

[13] Use of EBSD technique to examine microstructure and cracking in a bainitic steel, E. Bouyne, H.M. Flower, T.C. Lindley and A. Pineau, Scripta Materialia, Vol. 39, No. 3, pp. 295–300, 1998

[14] Texture Analysis with MTEX - Free and Open Source Software Toolbox, F. Bachmann, R. Hielscher, H. Schaeben: Solid State Phenomena (2010), 160, 63-68

[15] A.F. Gourgues, Electron backscatter diffraction and cracking, Materials science and technology, 18 (2002) 19